THE CATHOLIC UNIVERSITY OF AMERICA
DEPARTMENT OF ELECTRICAL ENGINEERING

DEVELOPMENT OF KINEMATIC EQUATIONS AND DETERMINATION OF WORKSPACE OF A 6 DOF END-EFFECTOR WITH CLOSED-KINEMATIC CHAIN MECHANISM

Charles C. Nguyen
Principal Investigator and Associate Professor
and
Farhad J. Pooran
Graduate Research Assistant

submitted to
Mr. David E. Provost
Code 735.1
Goddard Space Flight Center (NASA)
Greenbelt, Maryland

February 1989

SUMMARY

*This report presents the research results from the research grant entitled "*Active Control of Robot Manipulators*", funded by the Goddard Space Flight Center, under the Grant Number NAG 5-780, for the period between July 1, 1988 and January 1, 1989.*

In this report, we present the analysis of a 6 DOF robot end-effector built to study telerobotic assembly of NASA hardwares in space. Since the end-effector is required to perform high precision motion in a limited workspace, closed-kinematic chain mechanism is chosen for its design. A closed-form solution is obtained for the inverse kinematic problem and an iterative procedure employing Newton-Raphson method is proposed to solve the forward kinematic problem. A study of the end-effector workspace results in a general procedure for the workspace determination based on the link constraints. Computer simulation results are presented.

INTRODUCTION

Performing operations outside of life supporting environments such as the future NASA space station is considered to be a relatively hazardous task. Therefore, the concept of using space robots instead of astronauts for servicing and maintaining spacecrafts attracts tremendous robotic researchers' attention. Recognizing the above fact, NASA has focused on the research of *telerobotics*, a joining of *teleoperation* and *robotics* [1]. Teleoperation enables the human operator to perform tasks remotely in a shirtsleeve environment and robotics allows tasks, which are impossible to human control by teleoperation to be accomplished by a telerobot. Telerobotic operations can be performed either in a *traded control* mode (serial operation) or in a *shared control* mode (parallel operation). In the traded control mode, using teleoperation the human operator performs some portion of a task and then let the telerobot perform some other portion of the task autonomously. On the other hand, the human operator and the telerobot perform portions of the task simultaneously in a shared control mode. In either modes, successful robotic tasks require that the motion of the telerobot be controlled precisely. Robot motion can be categorized into gross motion and fine motion. While gross motion permits low position tolerances, e.g. in obstacle avoidance, fine motion requires a relatively high position tolerance, usually of thousands of an inch, e.g. in mating and fastening of parts. A telerobot system mainly consists of a master arm and a slave arm [Figure 1] which is a general open-kinematic chain (**OKC**) manipulator with six degrees of freedom (**DOF**) or more. During an assembly task, it is impractical to require the OKC manipulator to perform both gross and fine motion since OKC manipulators generally have poor performance in a fine motion operation. Therefore, the operation is more effective if a robotic end-effector possessing a capability of high precision positioning is mounted to the end of the OKC manipulator to perform fine and precise motion while the OKC manipulator performs only gross motion. The above distribution of tasks actually occurs in an operation performed in a traded control mode where the operator uses the master arm to move the OKC manipulator into the end-effector workspace in a gross motion mode and the end-effector will take over and perform the assembly autonomously in a fine motion mode.

Although OKC manipulators have large workspace and possess high dexterity, they are not used as high precision positioning devices because the cantilever-like structure causes the robot arm to have low stiffness. In addition, OKC manipulators have low vibrational frequencies due to the accumulation of effective masses associated with manipulator actuators and their open chain structure. In this kind of manipulators, large position error occurs at the last link because actuator errors accumulate throughout the OKC mechanism. Finally OKC manipulators have low strengh-to-weight ratios due to the fact that payloads are not uniformly distributed to the actuators. The above disadvantages of OKC manipulators have motivated active research of an alternative type of manipulators designed based on closed-kinematic chain mechanism (**CKCM**). A typical CKCM manipulator consists of two platforms driven by a number of parallel actuators and is often referred as *parallel mechanism* or *parallel manipulator*. Paying the price of relatively small workspace and low maneuverability, CKCM manipulators enjoy the high positionioning capability produced by their high structural rigidity and noncumulative actuator errors. CKCM manipulators also have higher strenght-to-weight ratios as compared to OKC manipulators because their actuators share the load proportionally. In summary, the CKCM is an ideal device for robotic tasks that require high precision motion within a limited workspace, e.g. in a fine motion mode of the telerobot end-effector.

Implementation of the CKCM concept first appeared in the design of the Stewart platform [2], originally designed as an aircraft simulator whose motion control problem was considered later in [3]. After its introduction, the Stewart platform mechanism attracted considerable researchers' interest and was proposed in many robotic applications [4,11]. New structural designs of robot arms based on the Stewart platform were proposed in [4] and motivated further development in [5]. A general technique was developed in [6] to describe the instantaneous link motion of a single closed-loop mechanism by employing linear algebra elements to screw systems. The author in [7] investigated the structural kinematic problem of in-parallel robot manipulators. A passive compliant robot end-effector was manufactured in [8] by utilizing the concept of Stewart platform mechanism whose kinematic problems and practical construction were later considered in [9] and [10], respectively. Investigation of inverse dynamic problem of platform-based manipulators was done in [11] and analysis of kinematics and dynamics of parallel manipulators was conducted in [12]. Dynamical equations for a 3 DOF CKCM and a 2 DOF CKCM manipulator were derived in [13] and [14], respectively by using the Lagrangian formulation.

Since CKCM is capable of performing high precision motion in a relatively small workspace, it is natural to propose that it be utilized in designing the end-effector to be mounted to the slave arm of the telerobot system to perform fine motion. As a consequence, a 6 DOF robot end-effector whose structure assumes a CKCM was recently designed and built to serve as a testbed for studying telerobotic assembly of NASA hardwares [8] in space. In this report, we first describe the main components of the CKCM end-effector. We then present the kinematic analysis which provides a closed-form solution to the inverse kinematic problem and an iterative procedure using Newton-Raphson method for the solution of the forward kinematic problem. Next we examine the workspace problem and then propose a general procedure for the determination of the reachable workspace for a set of link constraints. Computer simulation is then performed to demonstrate the procedure. Finally, evaluations and discussions of obtained results will conclude the report.

THE CKCM END-EFFECTOR

Figure 1 presents an artist's conception of a dual arm telerobot system consisting of a master system and slave system. The human operator uses the master arm to control the gross motion of the slave arm and the CKCM end-effectors mounted at the end of the two slave arms autonomously perform part assembly in a fine motion mode within its workspace. The end-effector should be manufactured such that it satisfies the requirements of compactness and lightweight. In order to study the performance of autonomous assembly of parts in a telerobotic operation, a 6 DOF end-effector whose size is about ten times that of the telerobot end-effector was designed and built at the Goddard Space Flight Center (**GSFC**) [8] and is currently located at the Center for Artificial Intelligence and Robotics (**CAIR**)[1]. As shown in Figure 2, the end-effector is a modified version of the Stewart platform, and mainly consists of an upper payload platform, a lower base platform and six linear actuators. The movable payload platform is supported above the stationary base platform by six axially entensible rods where recirculating ballscrews are used to provide the extensibility. Stepper motors were selected to drive the ballscrews to extend

[1]To test control schemes developed under a research grant with NASA/GSFC

or shorten the actuator lenghts whose variations will in turn produce the motion of the payload platform. Each end of the actuator links is mounted to the platforms by 2 rotary joints whose axes intersect and are perpendicular to each other. Therefore, the system has 24 rotary joints, 6 prismatic joints, and 14 links including the 2 platforms. Using the *number synthesis* [4], it can be shown that the CKCM end-effector possesses 6 degrees of freedom.

THE INVERSE KINEMATICS

In this section we first start developing the kinematic equation for a 6 DOF end-effector and then discuss the special cases of end-effectors having smaller number of degrees of freedom. Inverse kinematics deals with the determination of a set of joint variables, which yield a set of Cartesian variables, usually composed of Cartesian position and orientation of the end-effector with respect to some reference frame. For the CKCM end-effector, the lenghts of the links can be adjusted by the actuators, and therefore are chosen to be the joint variables. To define the Cartesian variables we proceed to assign two coordinate frames {**A**}, and {**B**} to the movable and base platforms, respectively. As Figure 3 illustrates, the origin of Frame {**A**} is chosen to be the centroid A of the payload platform, the $\mathbf{z}_A$-axis is pointing upward and the $\mathbf{x}_A$-axis passes through the joint attachment point A_1. The angle between A_1 and A_2 is denoted by θ_A, and in order to obtain a symmetrical distribution of joints on the payload platform the angles between A_1 and A_3 and between A_3 and A_5 are set to 120°. Similarly, Frame {**B**} has its origin at the centroid B of the base platform. The $\mathbf{x}_B$-axis passes through the joint attachment point B_1 and the angle between B_1 and B_2 is denoted by θ_B. Also the angles between B_1 and B_3 and between B_3 and B_5 are set to 120° so that a symmetrical distribution of joints on the base platform can be achieved. The Cartesian variables are chosen to be the relative position and orientation of Frame {**A**} with respect to Frame {**B**} where the position of Frame {**A**} is specified by the position of its origin with respect to Frame {**B**}. Now if we denote the angle between AA_i and $\mathbf{x}_A$ by λ_i, and the angle between BB_i and $\mathbf{x}_B$ by Λ_i for i=1,2,...,6, then by inspection we obtain

$$\Lambda_i = 60(i-1)^\circ;\ \lambda_i = 60(i-1)^\circ \ for\ i = 1,3,5 \tag{1}$$

and

$$\Lambda_i = \Lambda_{i-1} + \theta_B;\ \lambda_i = \lambda_{i-1} + \theta_A \ for\ i = 2,4,6. \tag{2}$$

Furthermore, if Vector ${}^A\mathbf{a}_i = (a_{ix}\ a_{iy}\ a_{iz})^T$ describes the position of the attachment point A_i with respect to Frame {**A**}, and Vector ${}^B\mathbf{b}_i = (b_{ix}\ b_{iy}\ b_{iz})^T$ the position of the attachment point B_i with respect to Frame {**B**}, then they can be written as

$${}^A\mathbf{a}_i = \begin{bmatrix} r_A cos(\lambda_i) & r_A sin(\lambda_i) & 0 \end{bmatrix}^T \tag{3}$$

and

$${}^B\mathbf{b}_i = \begin{bmatrix} r_B cos(\Lambda_i) & r_B sin(\Lambda_i) & 0 \end{bmatrix}^T \tag{4}$$

for i=1,2,...,6 where r_A and r_B represent the radii of the payload and base platforms, respectively.

We proceed to consider the vector diagram for an ith actuator given in Figure 4. The lenght vector ${}^B\mathbf{q}_i = (q_{ix}\ q_{iy}\ q_{iz})^T$, expressed with respect to Frame {**B**} can be computed by

$${}^B\mathbf{q}_i = {}^B\mathbf{a}_i - {}^B\mathbf{b}_i \tag{5}$$

where Vector ${}^B\mathbf{a}_i$ and Vector ${}^B\mathbf{d}$ describe the positions of A_i and A, respectively both in terms of Frame {B}. Vector ${}^B\mathbf{d}$ contains the Cartesian coordinates x, y, z of the origin, A of Frame {A} with respect to Frame {B} such that

$$ {}^B\mathbf{d} = \begin{pmatrix} x & y & z \end{pmatrix}^T . \tag{6} $$

Let ${}^B_A\mathbf{R}$ be the *Orientation Matrix*, which represents the orientation of Frame {A} with respect to Frame {B} and can be expressed as

$$ {}^B_A\mathbf{R} = \begin{bmatrix} r_{11} & r_{12} & r_{13} \\ r_{21} & r_{22} & r_{23} \\ r_{31} & r_{32} & r_{33} \end{bmatrix} \tag{7} $$

for i=1,2,...,6, then ${}^B\mathbf{a}_i$ can be computed by

$$ {}^B\mathbf{a}_i = {}^B_A\mathbf{R}\ {}^A\mathbf{a}_i + {}^B\mathbf{d}. \tag{8} $$

Now substituting (8) into (5) yields

$$ {}^B\mathbf{q}_i = {}^B_A\mathbf{R}\ {}^A\mathbf{a}_i + {}^B\mathbf{d} - {}^B\mathbf{b}_i \ for \ \text{i=1,2,...,6}, \tag{9} $$

which can be rewritten as

$$ {}^B\mathbf{q}_i = \begin{bmatrix} r_{11}a_{ix} + r_{12}a_{iy} + r_{13}a_{iz} + x - b_{ix} \\ r_{21}a_{ix} + r_{22}a_{iy} + r_{23}a_{iz} + y - b_{iy} \\ r_{31}a_{ix} + r_{32}a_{iy} + r_{33}a_{iz} + z - b_{iz} \end{bmatrix} . \tag{10} $$

Furthermore, the lenght of Vector ${}^B\mathbf{q}_i$, l_i can be computed from the vector components as

$$ l_i = \sqrt{q_{ix}^2 + q_{iy}^2 + q_{iz}^2}. \tag{11} $$

Employing (10), Equation (11) can be rewritten as

$$ \begin{aligned} l_i{}^2 \ = \ & x^2 + y^2 + z^2 + a_{ix}^2(r_{11}^2 + r_{21}^2 + r_{31}^2) + a_{iy}^2(r_{12}^2 + r_{22}^2 + r_{32}^2) \\ & + a_{iz}^2(r_{13}^2 + r_{23}^2 + r_{33}^2) + b_{ix}^2 + b_{iy}^2 + b_{iz}^2 + 2a_{ix}a_{iy}(r_{11}r_{12} + r_{21}r_{22} + r_{31}r_{32}) \\ & + 2a_{ix}a_{iz}(r_{11}r_{13} + r_{21}r_{23} + r_{31}r_{33}) + 2a_{iy}a_{iz}(r_{12}r_{13} + r_{22}r_{23} + r_{32}r_{33}) \\ & + 2(r_{11}a_{ix} + r_{12}a_{iy} + r_{13}a_{iz})(x - b_{ix}) + 2(r_{21}a_{ix} + r_{22}a_{iy} + r_{23}a_{iz})(y - b_{iy}) \\ & + 2(r_{31}a_{ix} + r_{32}a_{iy} + r_{33}a_{iz})(z - b_{iz}) - 2(xb_{ix} + yb_{iy} + zb_{iz}). \end{aligned} \tag{12} $$

From the properties of orientation matrix we have

$$ r_{11}^2 + r_{21}^2 + r_{31}^2 = r_{12}^2 + r_{22}^2 + r_{32}^2 = r_{13}^2 + r_{23}^2 + r_{33}^2 = 1 \tag{13} $$

and

$$ \begin{aligned} r_{11}r_{12} + r_{21}r_{22} + r_{31}r_{32} &= 0 \\ r_{11}r_{13} + r_{21}r_{23} + r_{31}r_{33} &= 0 \\ r_{11}r_{13} + r_{22}r_{23} + r_{32}r_{32} &= 0, \end{aligned} \tag{14} $$

and also from (1) and (2) we note that

$$a_{iz} = b_{iz} = 0 \tag{15}$$

and

$$a_{ix}^2 + a_{iy}^2 + a_{iz}^2 = r_A^2, \tag{16}$$

$$b_{ix}^2 + b_{iy}^2 + b_{iz}^2 = r_B^2. \tag{17}$$

Therefore, (12) can be simplified to

$$\begin{aligned} l_i^2 &= x^2 + y^2 + z^2 + r_A^2 + r_B^2 + 2(r_{11}a_{ix} + r_{12}a_{iy})(x - b_{ix}) \\ &\quad +2(r_{21}a_{ix} + r_{22}a_{iy})(y - b_{iy}) + 2(r_{31}a_{ix} + r_{32}a_{iy})z - 2(xb_{ix}), \end{aligned} \tag{18}$$

for i=1,2,...,6.

Equation (18) represents the solution to the inverse kinematic problem in the sense that for a given Cartesian configuration, composed of the position and orientation specified by (6) and (7), respectively, the actuator lengts l_i for i=1,2,...,6, can be computed using (18). We observe that nine variables are needed to describe the orientation of Frame $\{\mathbf{A}\}$ in Equation (7) and six of them are redundant because only three are needed to specify an orientation [18]. There exist several ways to represent an orientation by three variables, but the most widely used one is the Euler Angles α, β, and γ, which represent the orientation or Frame $\{\mathbf{A}\}$, obtained after the following sequence of rotations from Frame $\{\mathbf{B}\}$:

1. A rotation of α about the $\mathbf{z}_B$-axis (*Roll*)
2. A rotation of β about the $\mathbf{y}_B$-axis (*Pitch*)
3. A rotation of γ about the $\mathbf{x}_B$-axis (*Yaw*).

The orientation represented by α, β, and γ, is given by [2]

$$\mathbf{R}_{xyz}(\alpha,\beta,\gamma) = \begin{bmatrix} c\alpha\, c\beta & c\alpha\, s\beta\, s\gamma - s\alpha\, c\gamma & c\alpha\, s\beta\, c\gamma + s\alpha\, s\gamma \\ s\alpha\, c\beta & s\alpha\, s\beta\, s\gamma + c\alpha\, c\gamma & s\alpha\, s\beta\, c\gamma - c\alpha\, s\gamma \\ -s\beta & c\beta\, s\gamma & c\beta\, c\gamma \end{bmatrix}. \tag{19}$$

Figure 5 illustrates the application of the inverse kinematics in a joint-space control scheme where the desired position and orientation of the payload platform, specified by six variables x,y,z,α,β, and γ are converted to required actuator lenghts by using Equations (18) and (19), and to be compared with the actual lenghts measured by displacement sensors such as linear voltage differential transformers (**LVDT**), mounted along the actuator links.

Special Cases

We observe that the solution to the inverse kinematic problem presented by Equation (18) is expressed in term of the vectors ${}^A\mathbf{a}_i$ and ${}^B\mathbf{b}_i$, which depend on λ_i and Λ_i, respectively. To make the solution applicable to end-effectors which has a smaller number of degrees of freedom, we modify Equations (1) and (2), while preserving the symmetrical distribution of joints on the payload and base platforms to include the following cases:

[2] $c\alpha \equiv \cos\alpha$, and $s\alpha \equiv \sin\alpha$.

Even Number of DOF:

$$\Lambda_i = \frac{360}{n}(i-1)^o;\ \lambda_i = \frac{360}{n}(i-1)^o \ for\ i = odd. \tag{20}$$

and

$$\Lambda_i = \Lambda_{i-1} + \theta_B;\ \lambda_i = \lambda_{i-1} + \theta_A \ for\ i = even. \tag{21}$$

where n = 2,4,6, is the number of DOF and θ_A and θ_B are arbitrarily selected by the designer of the end-effector.

Odd Number of DOF:

$$\Lambda_i = \lambda_i = \frac{360}{n}(i-1)^o \ for\ i = 1,2,...,n \tag{22}$$

where n = 1,3,5, is the number of DOF and it is noted that in this case, $\theta_A = \theta_B = \frac{360}{n}$.

Investigations of several special cases were reported in [14] for 2 DOF, in [13] for 3 DOF and in [9] for 6 DOF, whose joint distributions all agree with (20)-(22).

THE FORWARD KINEMATICS

The forward kinematics deals with determining the position and orientation of the payload platform when the actuator lenghts l_i for i=1,2,...,6, are given. This situation often occurs in a Cartesian-space control scheme where the lenghts measured by the LVDT's are to be converted to the corresponding payload platform position and orientation which are then compared with the desired configuration specified by the user.

Let us consider Equation (9), in which the orientation matrix ${}^B_A\mathbf{R}$ is replaced by $\mathbf{R}_{xyz}(\alpha,\beta,\gamma)$ described in (19). In (9), if ${}^B\mathbf{q}_i$ were available, for i=1,2,...,6, then with 18 equations and 12 unknowns including r_{jk} for j=k=1,2,...,3, and x,y,z, the solution could be obtained in a closed-form expression. The orientation angles α,β,γ can then be found by solving the inverse kinematic problem of the Euler Angles [18]. However, since there exists no unique vector ${}^B\mathbf{q}_i$ for a given lenght l_i, the above approach is not feasible. In addition, sensors measuring Cartesian coordinates are not readily available while joint displacement sensors such as LVDT are usually *off-the-shelf* items. Consequently, in a practical situation, only the information of the actuator lenghts is available, and it leaves us no alternative but to apply Equation (18) to solve the forward kinematic problem.

The forward kinematic problem can be now formulated as to find a vector ${}^B\mathbf{d}$ (position) and a matrix $\mathbf{R}_{xyz}(\alpha,\beta,\gamma)$ (orientation) such that for a given set of l_i for i=1,2,...,6, Equation (18) holds. We recognize that it is a difficult, if not impossible task because we have to deal with a set of 6 highly nonlinear simultaneous equations with 6 unknowns. Similar to the inverse kinematics of OKC manipulators, generally there exists no closed-form solution for the forward kinematics of CKCM manipulators. It leads us to seek an iterative numerical method to solve the above set of nonlinear equations. One widely used technique for solving nonlinear equations has been the Newton-Raphson method [19], which is proposed in this section to solve the forward kinematic problem.

In order to apply the Newton-Raphson method, first we should define 6 scalar functions

$$f_i(\mathbf{a}) = 0 \ for\ \text{i=1,2,...,6} \tag{23}$$

where the vector **a** is defined as

$$\mathbf{a} = \begin{pmatrix} x & y & z & \alpha & \beta & \gamma \end{pmatrix}^T, \tag{24}$$

and then employ the iterative formula

$$\mathbf{a}_{k+1} = \mathbf{a}_k - [\mathbf{J}(\mathbf{a}_k)]^{-1}\, \mathbf{f}(\mathbf{a}_k) \tag{25}$$

where

$$\mathbf{f}(\mathbf{a}) = \begin{bmatrix} \mathbf{f}_1{}^T(\mathbf{a}) & \mathbf{f}_2{}^T(\mathbf{a}) & \mathbf{f}_3{}^T(\mathbf{a}) & \mathbf{f}_4{}^T(\mathbf{a}) & \mathbf{f}_5{}^T(\mathbf{a}) & \mathbf{f}_6{}^T(\mathbf{a}) \end{bmatrix}^T, \tag{26}$$

and the Jacobian matrix **J** of **f** is given by

$$\mathbf{J} = \begin{bmatrix} \frac{\partial \mathbf{f}_1}{\partial x} & \frac{\partial \mathbf{f}_1}{\partial y} & \frac{\partial \mathbf{f}_1}{\partial z} & \frac{\partial \mathbf{f}_1}{\partial \alpha} & \frac{\partial \mathbf{f}_1}{\partial \beta} & \frac{\partial \mathbf{f}_1}{\partial \gamma} \\ \frac{\partial \mathbf{f}_2}{\partial x} & \frac{\partial \mathbf{f}_2}{\partial y} & \frac{\partial \mathbf{f}_2}{\partial z} & \frac{\partial \mathbf{f}_2}{\partial \alpha} & \frac{\partial \mathbf{f}_2}{\partial \beta} & \frac{\partial \mathbf{f}_2}{\partial \gamma} \\ \vdots & \vdots & \vdots & \vdots & \vdots & \vdots \\ \frac{\partial \mathbf{f}_6}{\partial x} & \frac{\partial \mathbf{f}_6}{\partial y} & \frac{\partial \mathbf{f}_6}{\partial z} & \frac{\partial \mathbf{f}_6}{\partial \alpha} & \frac{\partial \mathbf{f}_6}{\partial \beta} & \frac{\partial \mathbf{f}_6}{\partial \gamma} \end{bmatrix} \tag{27}$$

until certain acceptable error is achieved.

The scalar functions specified by (23) can be found by rewriting (18) so that

$$\begin{aligned} x^2 + y^2 + z^2 + r_A^2 + r_B^2 + 2(r_{11}a_{ix} + r_{12}a_{iy})(x - b_{ix}) \\ +2(r_{21}a_{ix} + r_{22}a_{iy})(y - b_{iy}) + 2(r_{31}a_{ix} + r_{32}a_{iy})z - 2(xb_{ix}) - l_i{}^2 \;\; = \;\; 0, \end{aligned} \tag{28}$$

for i=1,2,...,6. The following algorithm summarizes the application of Newton-Raphson method in solving the forward kinematic problem

Algorithm 1

1. Select an initial guess $\mathbf{a}_1$.
2. Compute $\mathbf{f}_i(\mathbf{a}_1)$ for i=1,2,...,6 using (28).
3. Compute $\mathbf{J}(\mathbf{a}_1)$ using (27).
4. Compute $\mathbf{a}_2$ using (25).
5. Compute the difference between $\mathbf{a}_2$ and $\mathbf{a}_1$.
6. Repeat Steps 1–5 until an acceptable difference is obtained.

In Step 6, an acceptable error can be established by setting up a tolerance value T so that when the element e_i of the error vector **e** at the k iteration given by

$$\mathbf{e} = -J^{-1}\, f(\mathbf{a}_k) \tag{29}$$

satisfy

$$\sqrt{\sum_{i=1}^{6} e_i^2} \leq T. \tag{30}$$

To investigate the performance of the above algorithm, we implement it using a software package, called *System Simulation Language* (**SYSL**) on a PC AT to study the case in which the end-effector draws an ellipse defined by

$$\left(\frac{x}{5}\right)^2 + \left(\frac{y}{2.5}\right)^2 = 1 \ (in\ cm) \tag{31}$$

on a plane parallel to the base platform. The NASA end-effector parameters are $r_A = 0.7$m, $r_B = 0.8$m, $\theta_A = 30^o$, $\theta_B = 94^o$, $l_{min} = 40$inches, and $l_{max} = 53$inches. Here for simplicity, it is assumed that the payload platform frame $\{\mathbf{A}\}$ maintains a fixed orientation with respect to the base platform frame $\{\mathbf{B}\}$ while performing the motion. We first use the inverse kinematics to derive the actuator lenghts required for drawing the ellipse. The lenght information is then inputted to Algorithm 1 with a sampling rate of 10 Hz to obtain the Cartesian variables. The data obtained from the algorithm is plotted against the actual ellipse for comparision purpose. As Figure 5 shows, the proposed algorithm performs satisfactorily by providing relatively accurate information about the actual ellipse with minimal deviations. Its performance could be improved if the sampling rate is reduced and a faster computer is used. Real-time control of the end-effector requires that the sampling rate be at least 5 Hz [16]. Therefore, with a fast computer and a smaller number of iterations, Algorithm 1 can be implemented for converting lenght information into position and orientation in a real-time control problem. Successful implementation of Newton-Raphson method for real-time control with one iteration was reported in [3].

DETERMINATION OF WORKSPACE

Workspace analysis of CKCM end-effectors having 6 DOF or more is a difficult task due to fact that its spatial geometry of multiloop structure is highly complex, which results into the nonexistence of a closed-form solution for the forward kinematic problem. The reachable workspace of the end-effector depends on the maximum extension and shortening of the actuator lenghts and allowed ranges of joint rotation. In [9], the authors analyzed the reachable workspace of a 6 DOF manipulator with ball joints that are evenly distributed on both the platforms. They considered a special case in which the payload platform is allowed only to rotate about the **y**-axis, i.e. the rotations about the **x**-axis and **z**-axis are forbidden. As pointed out in [9], ball joints can only move freely with respect to all three Cartesian axes within the allowed ranges based on their physical dimension. As mentioned before, in the implementation the CKCM end-effector considered in this report, 2 rotary joints were utilized to connect each end of the actuator links to the platforms. Rotary joints were used instead of ball joints, because they require minimal maintenance and do not restrict the reachable workspace of the end-effector.

In this section we propose an algorithm that can be implemented to determine the reachable workspace of a general 6 DOF CKCM end-effector with rotary joints whose distributions on the platforms are arbitrary provided that a symmetrical distribution is preserved subject to (20)–(22). The algorithm employs both inverse and forward kinematic solutions and is given below:

Algorithm 2

1. Select a workspace bounded by the surface of a sphere whose origin is located at $[0\ 0\ (z_{max} - r_{min})]^T$ where r_{min}, the sphere radius is equal to $\frac{z_{max}-z_{min}}{2}$, z_{max}, the maximum vertical coordinate is obtained when all lenghts l_i for i=1,2,...,6 are extended to maximum values, and z_{min}, the minimum vertical coordinate is obtained when all lenghts l_i for i=1,2,...,6, are shortened to minimum values. The sphere selected here is the maximum sphere, on whose surface all points can be reached by the end-effector.

2. Use inverse kinematics to obtain the required lenghts of the surface of the sphere selected in Step 1.

3. Delete those points on the sphere surface, which correspond to lenghts that lie outside the allowed range specified by the lenght constraint, $l_{min} \leq l_i \leq l_{max}$.

4. Select another sphere whose radius r is equal to $r_m + \Delta r$, for $\Delta r \geq 0$.

5. Repeat Steps 1–4 until $r = r_{max}$ where r_{max} is the radius of the smallest sphere, on whose surface no point can be reached by the end-effector.

6. Plot the remaining space points in 2-dimensional or 3-dimensional coordinate systems.

To demonstrate the performance of Algorithm 2, we applied it to determine the reachable workspace of the NASA CKCM end-effector whose specifications were given in previous section. Algorithm 2 was implemented using SYSL and Matlab on a PC AT. The results are reported in Figures 7–9. Figure 7 shows the x-y plane projection of the reachable workspace while Figures 8 and 9 the x-z plane and y-z plane projections, respectively. As the figures show, the reachable workspace of the end-effector has the shape of a deformed football, which is as expected.

CONCLUSION

In this report we presented the kinematic analysis of a 6 DOF CKCM end-effector whose design was based on the mechanism of Stewart platform [2]. Since CKCM has high precision positioning capability within a limited workspace, we have proposed that the CKCM end-effector be mounted to the end of a telerobot to perform autonomous assembly of NASA hardwares in space. The kinematic analysis of the end-effector was performed and resulted in a closed-form solution for the inverse kinematic problem so that required lenghts can be computed for a given Cartesian configuration. Newton-Raphson method was employed to treat the forward kinematic problem whose solution can be obtained iteratively using a proposed algorithm (Algorithm 1). Determination of the end-effector workspace was also considered and an algorithm (Algorithm 2) was provided to compute the reachable workspace of a general CKCM end-effector. Computer simulation was conducted to investigate the proposed algorithms. Future research can be extended to studying the dynamics of CKCM end-effectors [15] and control schemes for controlling position and force [16] of this type of robot end-effectors.

References

[1] JPL, "Telerobotics Project Plan," *Jet Propulsion Laboratory*, JPL D-5692, August 1988.

[2] Stewart, D., "A Platform with Six Degrees of Freedom," *Proc. Institute of Mechanical Engineering*, vol. 180, part 1, No. 5, pp. 371-386, 1965-1966.

[3] Dieudonne, J.E. et al, "An Actuator Extension Transformation for a Motion Simulator and an Inverse Transformation Applying Newton-Raphson's Method," *NASA Technical Report D-7067*, 1972.

[4] Hunt, K. H., *Kinematic Geometry of Mechanisms*, Oxford University, London 1978.

[5] Fichter, E.F. and MacDowell, E.D., "A Novel Design for a Robot Arm," *ASME Int. Computer Technology Conference*, San Francisco, pp. 250-256, 1980

[6] Sugimoto, K. and Duffy, J., "Application of Linear Algebra to Screw Systems," *Mech. Mach. Theory*, Vol. 17, No. 1, pp. 73-83, 1982.

[7] Hunt, K. H., "Structural Kinematics of in-parallel-actuated Robot Arms," *Trans. ASME, J. Mech., Transmis., Automa. in Des.*, Vol. 105, pp. 705-712, 1983.

[8] Premack, Timothy et al, "Design and Implementation of a Compliant Robot with Force Feedback and Strategy Planning Software," *NASA Technical Memorandum 86111*, 1984.

[9] Yang, D. C. and Lee, T. W., "Feasibility Study of a Platform Type of Robotic Manipulators from a Kinematic Viewpoint," *Trans. ASME Journal of Mechanisms, Transmissions, and Automation in Design*, Vol. 106. pp. 191-198, June 1984.

[10] Fichter, E.F., "A Stewart Platform-Based Manipulator: General Theory and Practical Construction," *Int. Journal of Robotics Research*, pp. 157-182, Summer 1986

[11] Do, W.Q.D. and Yang, D.C.H., "Inverse Dynamics of a Platform Type of Manipulating Structure," *ASME Design Engineering Technical Conference*, Columbus, Ohio, pp. 1-9, 1986.

[12] Sugimoto, K., "Kinematic and Dynamic Analysis of Parallel Manipulators by Means of Motor Algebra," *ASME Journal of Mechanisms, Transmissions, and Automation in Design*, pp. 1-5, Dec. 1986.

[13] Lee, K. M., Chao, A., and Shah, D. K., "A Three Degrees of Freedom In-parallel Actuated Manipulator," *Proc. IASTED Int. Conf.*, pp. 134-138, 1986.

[14] Nguyen, C. C., Pooran, F.J. and Premack, T., "Trajectory Control of Robot Manipulator with Closed-Kinematic Chain Mechanism," *Proc. 20th Southeastern Symposium on System Theory*, North Carolina, pp. 454-458, March 1988.

[15] Nguyen, C.C., Pooran, F.J., "Kinematics and Dynamics of a Six-Degree-of-Freedom Robot Manipulator with Closed-Kinematic Chain Mechanism," in *Robotics and Manufacturing: Recent Trends in Research, Education, and Application*, Chapter 7, edited by M. Jamshidi et al, ASME Press, New York, pp. 351-359, 1988.

[16] Nguyen, C.C., Pooran, F.J., "Adaptive Control of Robot Manipulators with Closed-Kinametic Chain Mechanism," in *Robotics and Manufacturing: Recent Trends in Research, Education, and Application*, Chapter 4, edited by M. Jamshidi et al, ASME Press, New York, pp. 177-186, 1988.

[17] Behi, F., "Kinematic Analysis for a Six-Degree-of-Freedom 3-PRPS Parallel Mechanism," *IEEE Journal of Robotics and Automation*, Vol. 5, No. 5, pp. 561-565, October 1988.

[18] Fu, K.S. et.al., *Robotics: Control, Sensing, Vision, and Intelligence* , McGraw-Hill, New York, 1987.

[19] Chua, L.O., Lin, P.M., *Computer-Aided Analysis of Electronic Circuits*, Prentice-Hall, New Jersey, 1975.

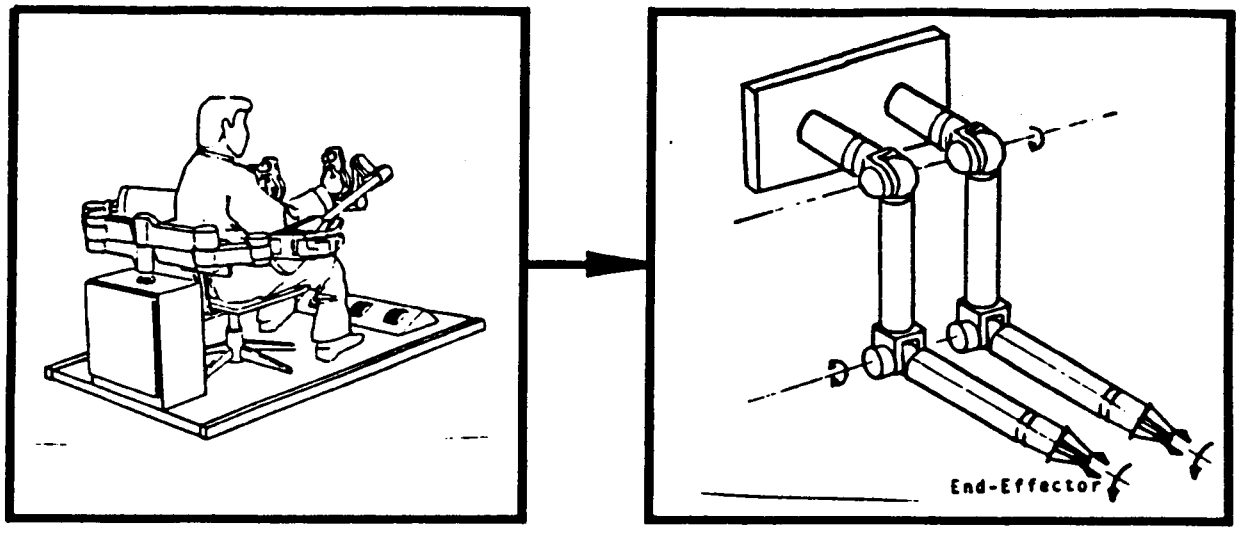

MASTER SYSTEM
(HUMAN OPERATOR)

SLAVE SYSTEM
(DUAL ARM)

Figure 1: A telerobot system with CKCM end-effectors

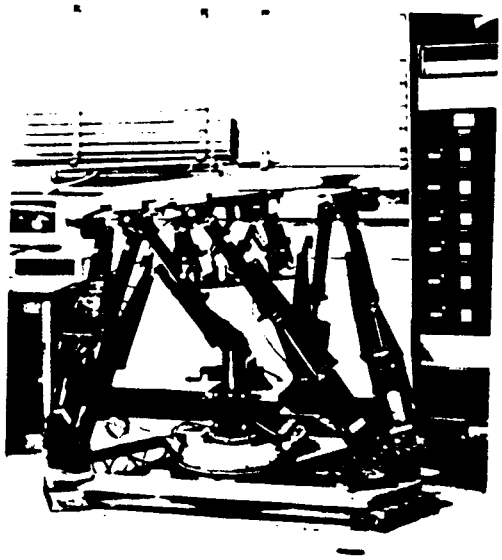

Figure 2: The CKCM end-effector.

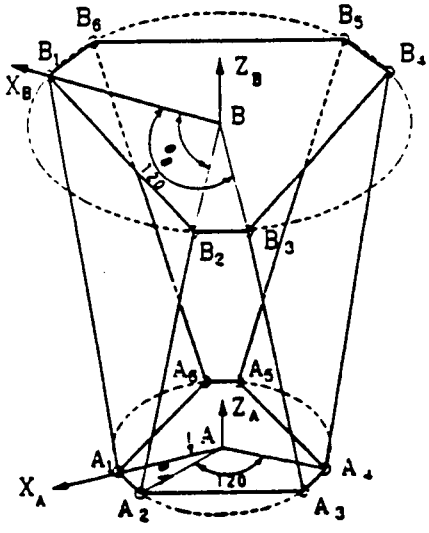

Figure 3: Platform frame assignment.

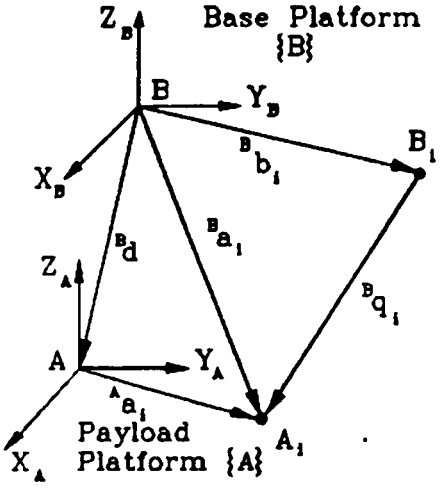

Figure 4: Vector diagram for ith actuator.

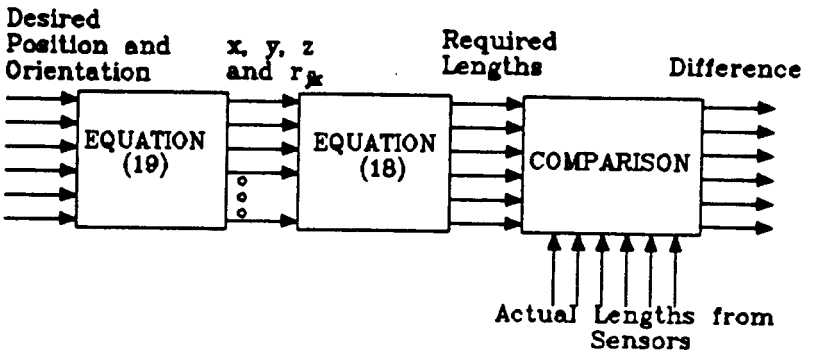

Figure 5: Joint-space control scheme.

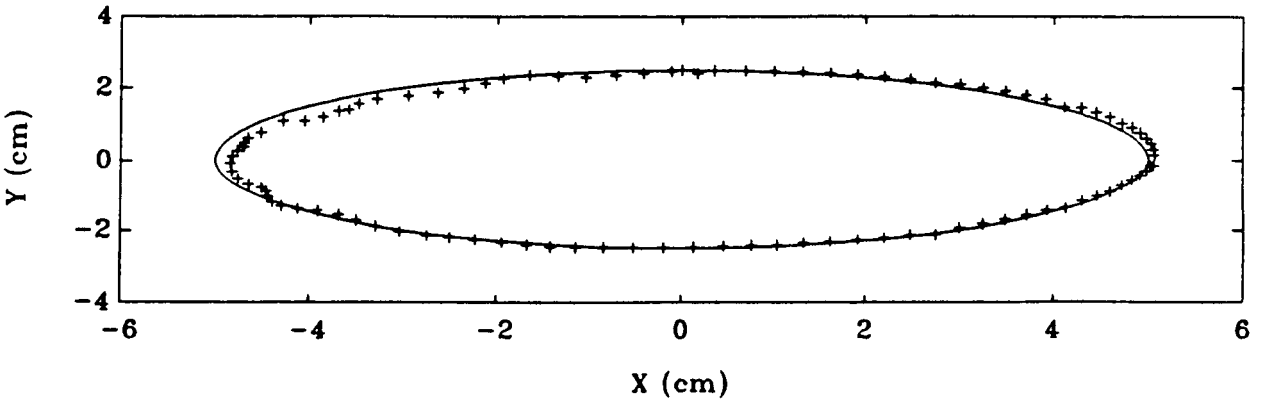

Figure 6: Demonstration of forward kinematic solution.
(*solid line*: actual value; *crossed line*: computed value)

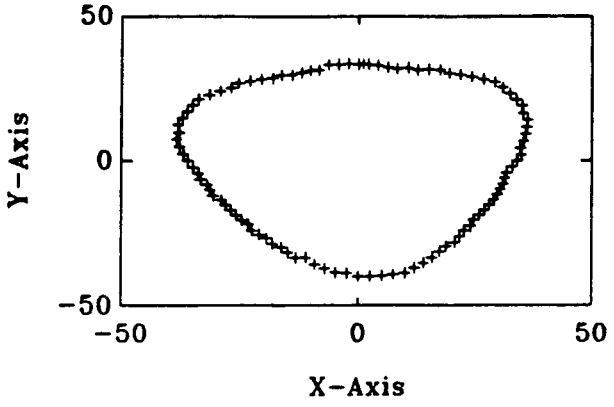

Figure 7: The x-y plane.

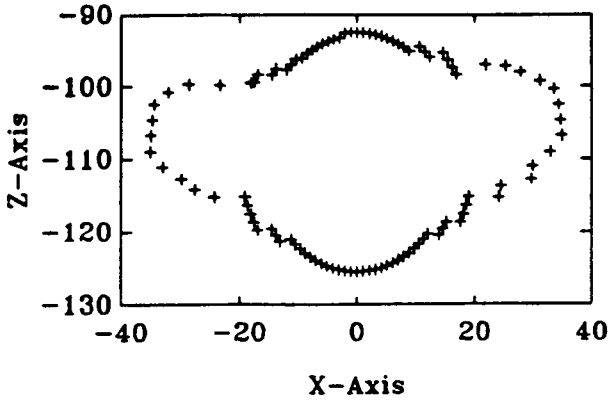

Figure 8: The x-z plane.

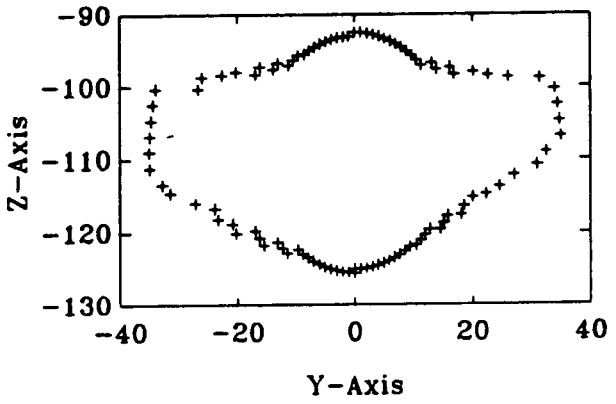

Figure 9: The y-z plane.